Vertical plasmonic resonance coupler

Yi-Jang Hsu and Yinchieh Lai*

Department of Photonics & Institute of Electro-Optical Engineering, National Chiao-Tung University, Hsinchu 300, Taiwan

yclai@mail.nctu.edu.tw

Abstract: Efficient wavelength-selective coupling of lights between sub-wavelength plasmonic waveguides and free space is theoretically investigated. The idea is based on a new type of vertical resonance coupling devices built on plasmonic metal/insulator/metal (MIM) waveguides. The device structure consists of a vertical grating coupler in a resonance cavity formed by two distributed Bragg reflectors (DBRs). With the metal loss included, maximum coupling efficiency around 50% can be obtained at the 1550 nm wavelength with a filtering 3dB bandwidth around 20 nm (7nm for the lossless case), demonstrating the feasibility of the idea for achieving high efficiency wavelength-selective vertical coupling through optical resonance. By utilizing this coupler, a plasmonic add-drop device is proposed and theoretically demonstrated. This kind of compact wavelength selective coupling devices shall have the potential to open up a new avenue of photonics circuitry at nanoscale.

OCIS codes: (240.6680) Surface plasmons; (130.3120) Integrated optics devices; (050.2770) Gratings; (050.6624) Subwavelength structures; (060.1810) Buffers, couplers, routers, switches, and multiplexers; (250.5403) Plasmonics.

References and links

1. W. L. Barnes, A. Dereux, and T. W. Ebbesen, "Surface plasmon subwavelength optics," Nature **424**(6950), 824–830 (2003).
2. S. I. Bozhevolnyi, V. S. Volkov, E. Devaux, J. Y. Laluet, and T. W. Ebbesen, "Channel plasmon subwavelength waveguide components including interferometers and ring resonators," Nature **440**(7083), 508–511 (2006).
3. R. F. Oulton, V. J. Sorger, T. Zentgraf, R. M. Ma, C. Gladden, L. Dai, G. Bartal, and X. Zhang, "Plasmon lasers at deep subwavelength scale," Nature **461**(7264), 629–632 (2009).
4. Z. Fang, Q. Peng, W. Song, F. Hao, J. Wang, P. Nordlander, and X. Zhu, "Plasmonic focusing in symmetry broken nanocorrals," Nano Lett. **11**(2), 893–897 (2011).
5. C. M. Chang, M. L. Tseng, B. H. Cheng, C. H. Chu, Y. Z. Ho, H. W. Huang, Y. C. Lan, D. W. Huang, A. Q. Liu, and D. P. Tsai, "Three-dimensional plasmonic micro projector for light manipulation," Adv. Mater. **25**(8), 1118–1123 (2013).
6. S. M. Nie and S. R. Emory, "Probing single molecules and single nanoparticles by surface-enhanced Raman scattering," Science **275**(5303), 1102–1106 (1997).
7. T. W. Ebbesen, C. Genet, and S. I. Bozhevolnyi, "Surface plasmon circuitry," Phys. Today **61**(5), 44–50 (2008).
8. B. H. Cheng and Y. C. Lan, "Multi-layered dielectric cladding plasmonic microdisk resonator filter and coupler," Phys. Plasmas **20**(2), 020701 (2013).
9. S. A. Maier, *Plasmonics: Fundamentals and Applications* (Springer, 2007).
10. J. P. Tetienne, A. Bousseksou, D. Costantini, Y. De Wilde, and R. Colombelli, "Design of an integrated coupler for the electrical generation of surface plasmon polaritons," Opt. Express **19**(19), 18155–18163 (2011).
11. S. Ura, S. Murata, Y. Awatsuji, and K. Kintaka, "Design of resonance grating coupler," Opt. Express **16**(16), 12207–12213 (2008).
12. G. Roelkens, D. Van Thourhout, and R. Baets, "High efficiency grating coupler between silicon-on-insulator waveguides and perfectly vertical optical fibers," Opt. Lett. **32**(11), 1495–1497 (2007).
13. K. Kintaka, Y. Kita, K. Shimizu, H. Matsuoka, S. Ura, and J. Nishii, "Cavity-resonator-integrated grating input/output coupler for high-efficiency vertical coupling with a small aperture," Opt. Lett. **35**(12), 1989–1991 (2010).
14. Y. Zhou, M. Moewe, J. Kern, M. C. Y. Huang, and C. J. Chang-Hasnain, "Surface-normal emission of a high-Q resonator using a subwavelength high-contrast grating," Opt. Express **16**(22), 17282–17287 (2008).
15. X. F. Li, S. F. Yu, and A. Kumar, "A surface-emitting distributed-feedback plasmonic laser," Appl. Phys. Lett. **95**(14), 141114 (2009).

#223864 - $15.00 USD Received 26 Sep 2014; revised 15 Dec 2014; accepted 17 Dec 2014; published 7 Jan 2015

16. S. Ura, H. Moriguchi, S. Kido, T. Suhara, and H. Nishihara, "Switching of output coupling in a grating coupler by diffraction transition to the distributed Bragg reflector regime," Appl. Opt. **38**(12), 2500–2503 (1999).
17. K. Kintaka, J. Nishii, Y. Imaoka, J. Ohmori, S. Ura, R. Satoh, and H. Nishihara, "A guided-mode-selective focusing grating coupler," IEEE Photon. Technol. Lett. **16**(2), 512–514 (2004).
18. H. Zhang and H. P. Ho, "Low-loss plasmonic waveguide based on gain-assisted periodic metal nanosphere chains," Opt. Express **18**(22), 23035–23040 (2010).
19. Y. Kou, F. Ye, and X. Chen, "Low-loss hybrid plasmonic waveguide for compact and high-efficient photonic integration," Opt. Express **19**(12), 11746–11752 (2011).
20. J. B. Khurgin and G. Sun, "Practicality of compensating the loss in the plasmonic waveguides using semiconductor gain medium," Appl. Phys. Lett. **100**(1), 011105 (2012).
21. Y. T. Wang, B. H. Cheng, Y. Z. Ho, Y. C. Lan, P. G. Luan, and D. P. Tsai, "Gain-assisted hybrid-superlens hyperlens for nano imaging," Opt. Express **20**(20), 22953–22960 (2012).
22. H. A. Haus, *Waves and Fields in Optoelectronics* (Prentice, 1984).
23. J. Ohmori, Y. Imaoka, S. Ura, K. Kintaka, R. Satoh, and H. Nishihara, "Integrated-optic add/drop multiplexing of free-space waves for intra-board chip-to-chip optical interconnects," Jpn. J. Appl. Phys. **44**(11), 7987–7992 (2005).
24. K. Kintaka, J. Nishii, K. Shinoda, and S. Ura, "WDM signal transmission in a thin-film waveguide for opitcal interconnection," IEEE Photon. Technol. Lett. **18**(21), 2299–2301 (2006).
25. H. A. Haus and Y. Lai, "Theory of cascaded quarter wave shifted distributed feedback resonators," IEEE J. Quantum Electron. **28**(1), 205–213 (1992).
26. W. Lin and G. P. Wang, "Metal heterowaveguide superlattices for a plasmonic analog to electronic Bloch oscillations," Appl. Phys. Lett. **91**(14), 143121 (2007).

1. Introduction

In recent years the surface plasmon polariton (SPP) structures [1] have attracted intensive investigation both theoretically and experimentally due to their unique properties. In these structures, lights propagating along the metal-dielectric surface are strongly confined with exponentially decaying fields away from the interface, which in principle can lead to the miniaturization of photonic devices and circuits down to the nanometer scale. By manipulating the geometric and material parameters of the metal-dielectric surfaces, various applications in subwavelength waveguiding [2], light generation [3], focusing [4, 5], and biomedical plasmonics [6] have been investigated. Thanks to the advances of related technologies, modern nano-fabrication and characterization techniques have experienced huge improvement with regards to the structured metal surfaces. It is expected that the SPP-based waveguides can offer the possibility for reducing the device structure down to the nanometer scale. The SPP-based photonic circuitry may also offer an effective solution to merge photonics and electronics when implementing future photonic systems based on optical fibers and photonic integrated circuits [7]. Stimulated by this plasmonic optoelectronic circuit concept, many passive and active plasmonic devices such as waveguides, couplers, filters, switches and light sources have been demonstrated [8]. However, due to their nanoscale field confinement characteristics, the light coupling issues between the sub-wavelength plasmonic waveguides and the free space are still challenging in many applications.

In the literature, there have been many reported research works for achieving efficient excitation of the SPP waveguide modes. Adiabatic mode conversion based on tapering device structures for improving mode mismatch is one of the fundamental approaches that have been widely used. However, many reported results were still performed on the larger confinement cases [9]. For geometries below the diffraction limit, such as MIM waveguides with a deep sub-wavelength dielectric core, the coupling efficiency is still low due to the small overlap between the excitation beam and the SPP waveguide mode [10]. On the other hand, the grating coupler (GC) is another approach that has been widely used for coupling between a guided wave and a free-space propagated wave. Vertical coupling can be achieved through proper phase matching design and the mode mismatch issue can be greatly reduced due to the enlarged grating coupling region. A vertical GC can thus provide many functions such as the far-field observation of a guided wave [11] and the vertical light coupling between different optical devices [12, 13]. The approach has also been utilized in implementing new light sources [14, 15], optical switches [16], and guided-mode selectors [17].

#223864 - $15.00 USD Received 26 Sep 2014; revised 15 Dec 2014; accepted 17 Dec 2014; published 7 Jan 2015

The resonance grating coupler concept previously developed for dielectric waveguides [12, 13] is an interesting one. High coupling efficiency as well as wavelength-selective coupling can be simultaneously achieved through the optical resonance effects. In this work, we investigate a plasmonic resonance grating coupler structure particularly designed for sub-wavelength MIM SPP waveguides, with the anticipation for achieving efficient wavelength-selective optical coupling in a small footprint. Ideally 100% coupling is possible if the device is lossless, as predicted by the coupled mode theory. We demonstrate a designed example that can reach 94% vertical coupling efficiency under the lossless condition. This corresponds to the optimal performance if the intrinsic metal loss of plasmonic waveguides could be overcome by some active means [18–21]. The vertical coupling efficiency can still reach around 50% even when reasonable metal loss is included, which corresponds to the practical coupling efficiency that can be achieved for passive devices. After the introduction given in this section (Section 1), the physical principles and design considerations for the studied device structure are described in Section 2. In particular, the coupled mode theory in time [22] is used to explain why the ideal 100% coupling efficiency could be achieved if the metal loss can be overcome. In Section 3, the Finite Difference Time Domain (FDTD) numerical method is utilized to simulate the performance of the designed device. In Section 4, an ultra-compact plasmonic add-drop device composed of two vertical plasmonic resonance couplers is proposed. The footprint of the novel add-drop device is thousands of times smaller than the dielectric devices [23, 24]. It has the potential to perform coarse wavelength division optical channel add/drop functionality [25] for SPP-based photonic integrated circuits. Finally in Section 5, we give a brief conclusion about the whole study.

2. Wavelength-selective vertical coupling by optical resonance

The schematic of the proposed plasmonic vertical coupler is depicted in Fig. 1. A GC formed by refractive index modulation on one cladding side of the metal-insulator-metal (MIM) waveguide is inserted between a front and a rear MIM distributed Bragg reflectors (DBRs) with refractive index modulation on both cladding sides. The optical wave is guided in the y-direction, propagates in the *x*-direction, and the whole structure is assumed to be uniform in the *z*-direction for the modeling simplicity. The right DBR is with longer length to totally reflect the light at the Bragg wavelength while the left DBR is with shorter length so that it also functions as an input/output coupling port. The other input/output coupling port is through the GC.

Some important design considerations are explained below. The grating period of the center GC section is determined by the phase-matching condition stated in (1). The forward/backward propagated MIM waveguide modes with the propagation vector $\vec{K}$ are phase-matched to the vertically propagated free space wave through the first order diffraction. This is how vertical coupling can be achieved through a properly designed waveguide grating coupler. However, as stated in (2), the second order diffraction effect of the GC will also couple the forward and backward propagated MIM waveguide modes directly, which will produce additional wave reflection effects

$$\overrightarrow{K_{GC}} + \vec{K} = 0 \left(\text{first order}\right) \tag{1}$$

$$2 * \overrightarrow{K_{GC}} + \vec{K} = -\vec{K} \left(\text{second order}\right) \tag{2}$$

On the other hand, the grating periods of the front and rear DBRs are properly determined to produce Bragg reflection at the same operation wavelength according to the formula $\left\|\overrightarrow{K_{DBR}}\right\| / 2 = \left\|\vec{K}\right\|$. Most importantly, when the GC is inserted between the two DBRs, the two phase shift spaces(L_F, L_R) between the GC and the two DBRs need to be properly adjusted so as to avoid unnecessary resonances. This is because the second order diffraction

#223864 - $15.00 USD Received 26 Sep 2014; revised 15 Dec 2014; accepted 17 Dec 2014; published 7 Jan 2015

effects of the center GC section will also produce wave reflection as explained above, which may cause unwanted resonances after reflecting back by the DBRs. By inserting additional phase shifts to enforce destructive interference for these unwanted resonances, one can make sure the resonance occurred at the operation wavelength is only caused by the cavity formed by the two DBRs. Compared to previous dielectric cases [11, 12], one important difference of the current plasmonic device structure is that we only need to put the index modulation on one cladding side of the GC for achieving high coupling efficiency. An additional reflection mirror is required for the dielectric cases to enforce light output in one port [13]. Such a disadvantage has been completed avoided in the current plasmonic device.

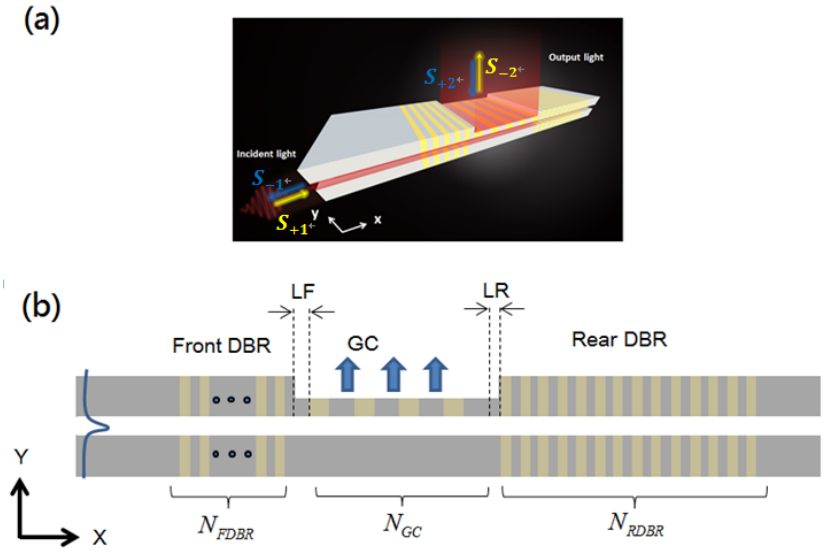

Fig. 1. (a) Schematic of the proposed vertical plasmonic resonance coupler. (b) The cross section of the device: the core of MIM waveguide is 15 nm. The period of the DBR (Λ_{DBR}) is 0.46 μm with the ε_{mL} material (tan area) width = 0.27 μm. The length of front DBR is 2.3 μm (= 5 Λ_{DBR}, Λ_{DBR}, N_{FDBR} = 5) for lossless case and 1.38 μm (= 3 Λ_{DBR}, N_{FDBR} = 3) for loss case. The length of rear DBR is 6.44 μm (= 14 Λ_{DBR}). The period of the GC (Λ_{GC}) is 0.983 μm with the ε_{mL} material (tan area) width = 0.577 μm and thickness = 0.0125 μm. The length of the GC is 3.932 μm (= 4 Λ_{GC}). The LF and LR are 0.02 μm and 0.37 μm, respectively.

If the device is designed by following the above considerations carefully, the main optical resonance in the device is defined by the cavity formed by the two DBRs and the GC will mainly function as an output coupler. The whole device can be considered as a single resonator directly coupled to two input/output ports as illustrated in Fig. 1(a). Within the framework of the coupled mode theory in time, the optical field in the resonator will evolve according to [22]:

$$\frac{da}{dt} = j\omega_o a - (\frac{1}{\tau_0} + \frac{1}{\tau_{e1}} + \frac{1}{\tau_{e2}})a + \sqrt{\frac{2}{\tau_{e1}}}S_{+1} + \sqrt{\frac{2}{\tau_{e2}}}S_{+2} \qquad (3)$$

Here ω_o is the resonance frequency, $1/\tau_0$ is the decay rate due to internal loss and $1/\tau_{e1}, 1/\tau_{e2}$ are the decay rates due to external coupling. The left incident wave is marked as S_{+1} and the

#223864 - $15.00 USD Received 26 Sep 2014; revised 15 Dec 2014; accepted 17 Dec 2014; published 7 Jan 2015

right incident wave is marked as S_{+2}. The output waves of the two ports are marked as S_{-1} and S_{-2} respectively, which can be calculated according to

$$S_{-i} = -S_{+i} + \sqrt{2/\tau_{ei}}\, a, \quad i = 1, 2 \tag{4}$$

If there is only one single-frequency incidence wave at port 1 with the frequency ω, one can obtain the following relation for the output wave at port 2:

$$S_{-2} = \frac{\sqrt{2/\tau_{e1}}\sqrt{2/\tau_{e2}}}{j(\omega-\omega_0) + (1/\tau_0 + 1/\tau_{e1} + 1/\tau_{e2})} S_{+1} \tag{5}$$

Therefore, the power transmission from port 1 to port 2 is:

$$\left\|S_{-2}\right\|^2 = \frac{(\frac{4}{\tau_{e1}\tau_{e2}})}{(\omega-\omega_0)^2 + 1/\tau^2} \left\|S_{+1}\right\|^2 \tag{6}$$

with $1/\tau = (1/\tau_0 + 1/\tau_{e1} + 1/\tau_{e2})$. One can see that the ideal 100% transmission can occur at resonance $(\omega = \omega_0)$ when there is no internal loss $1/\tau_0 = 0$ and the two ports are symmetric $(1/\tau_{e1} = 1/\tau_{e2})$. This simple derivation provides the theoretical basis to achieve high coupling efficiency based on the studied device structure. It should be noted that the present analysis based on the coupled mode equations in the time domain is approximate in the sense that all the spatial mode details have been reduced into a few coefficients (i.e., resonance frequencies and decay rates due to internal loss & external coupling). We simply utilize this theory to prove the possibility of achieving high coupling efficiency (ideally 100%) for the proposed device structure and do not try to evaluate these coefficients for performance analysis. The actual performance analysis is resorted to the direct FDTD simulation presented in the next section, so that all the wave propagation effects can be included in the calculation without approximation.

3. Numerical simulation results

By choosing appropriate parameters, we have designed an example device structure to operate at the wavelength of 1550 nm. The transmission spectra obtained by 2D FDTD simulation are illustrated in Fig. 2(a). The dielectric property of the metal cladding is modeled by the Drude formula:

$$\varepsilon_m(\omega) = 1 - \omega_p{}^2 / (\omega^2 + i\omega\gamma) \tag{7}$$

Here ω_p and γ are the plasma frequency and the decay rate respectively. For forming grating structures by index modulation, we will assume that there are two kinds of metallic materials can be used: one with $\omega_{pL} = 20\ eV$, $\gamma_{pL} = 0.01\ eV$ and the other with $\omega_{pH} = 9\ eV$, $\gamma_{pH} = 0.001\ eV$ [26]. We will denote ε_{mL} and ε_{mH} to be the dielectric constants of the two metals with low and high indices respectively. Similarly, ε_d is the dielectric constant of the MIM waveguide in the core region. For the ideal lossless case, one can simply set $\gamma = 0$. The two DBRs have the same period of 0.46 μm and the width for the ε_{mH} material is 0.27 μm. The reflection and transmission spectra of the rear Bragg reflector is also shown in the inset of Fig. 2(a) with $N_{RDBR} = 14$ periods to get total reflection. For operating at 1550 nm, the period of GC is chosen to be 0.983 μm. The width for the ε_{mL} material is 0.577 μm and the thickness is 0.0125 μm. For minimizing the device size, a small

#223864 - $15.00 USD Received 26 Sep 2014; revised 15 Dec 2014; accepted 17 Dec 2014; published 7 Jan 2015

aperture of vertical coupling is adopted. The total length of GC is 4 Λ_{GC} (N_{GC} = 4) such that the output coupling is still strong enough with the high contrast of the metal grating. When the GC is inserted between the rear DBR and front DBR, the two phase shift lengths (L_F , L_R) are set to be 0.02 μm and 0.37 μm respectively. The reflection of the front DBR should also be fine-tuned to optimize the net transmission at the operation wavelength. For the ideal lossless case, the net vertical transmission can be demonstrated to be as high as 94% as shown in Fig. 2(a), which is already close to the 100% theoretical limit. To demonstrate vertically light propagation from the free space port of the device, the E_x field distribution at 1550 nm is shown in Fig. 2(b), in which the 90 degree free space out-coupling can be clearly seen. With the metal loss included, the design is changed from $N_{FDBR} = 5$ to $N_{FDBR} = 3$ for maximum coupling and the net transmission spectrum is also plotted in Fig. 2(a) (the black line). The maximum transmission can still be close to 50% as demonstrated by the considered design example.

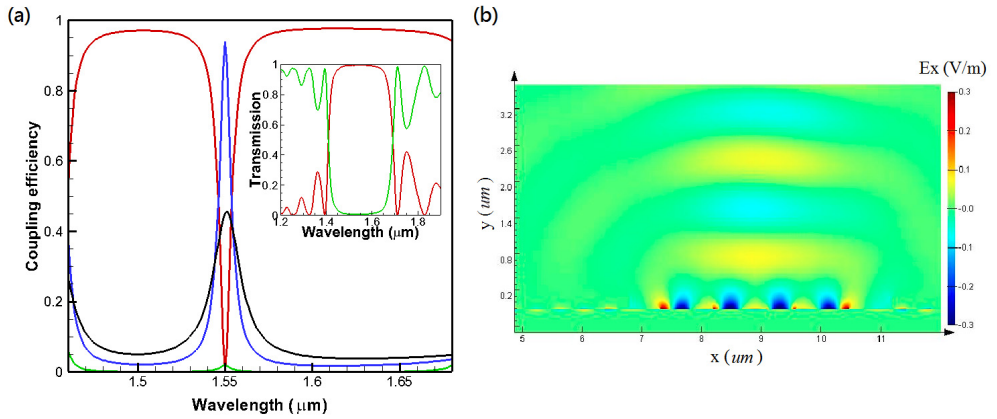

Fig. 2. (a) Vertical coupling efficiency and refection spectra of the whole device under lossless condition. Red: Reflection, Green: Transmission, and Blue: coupling to free space for the lossless case, Black: coupling to free space when loss is included. The inset: Reflection spectrum of the rear DBR individually. (b) Simulated E_x field distribution at the wavelength of 1550 nm.

In Fig. 2(b), it can be noted that when the light is coupled out of the free space port, the diffraction effect of free space propagation occurs and the wave fronts become curved gradually, since the beam size is only around 3 micro-meter in our design. When the free space coupling distance is long, this diffraction effect may produce additional optical mode-mismatch loss for optical coupling. In principle, one can reduce the effect by increasing the beam size or by decreasing the coupling distance. In our design example, we try to keep the device size smaller and thus choose the 3 micro-meter beam size for demonstration. If the device size is not a concern, the effect can be much more reduced by adopting a larger beam size.

From the numerical studies, we have found that the most sensitive physical quantity is the center wavelength of the device. Other physical quantities like bandwidth, reflectivity, and coupling efficiency are much less sensitive to the device parameters. This is because the center wavelength is determined by the resonance condition of the DBR cavity. The changes of the width and/or thickness parameters will slightly change the effective propagation constant of the waveguide and thus the resonance wavelength will also be changed. We have performed the sensitivity analyses for some of the parameters to estimate the implementation difficulties. The thickness of the GC layer is one of the most critical parameters. From our numerical simulation, the sensitivity ratio between the center wavelength change (in nm) and this thickness change (in nm) is around 10 for our design example. With today's technologies

#223864 - $15.00 USD Received 26 Sep 2014; revised 15 Dec 2014; accepted 17 Dec 2014; published 7 Jan 2015

one already can grow 10 nm Ag layer thicknesses with ± 0.5nm deviation. Thus it is reasonable to expect that one should be able to control the center wavelength of the device to the 10 nm order with today's technologies, which should be adequate for experimentally demonstrating the device. With more push of the technologies, more optimization of the design, and more development of the possible post fine-tuning processes, one might be able to push the control accuracy down to the nm order, which should be adequate for some applications. The sensitivity analyses for other critical parameters reach similar conclusions. We thus believe that the device structure is not totally out of the reach for practical implementation.

Some more details about the performed numerical simulation can also be given below. The grid sizes in the x and y dimensions are both 3.5 nm for calculating the presented results. The perfect matched layer (PML) absorbing boundary condition and the dielectric volume average method are used along with the FDTD simulation. We have found that if the grid size is further reduced, the center wavelength of the device will be somewhat shifted, possibly due to the slightly change of the calculated effective propagation constant of the optical waveguide. The other physical quantities (bandwidth, reflectivity, coupling efficiency, etc.) will basically remain the same. By slightly changing the length parameters, it is easy to shift the center wavelength back to the designed wavelength and obtain basically the same spectra. With such confirmation, we believe the presented results here should be a trustable numerical demonstration for the achievable device performance.

4. Plasmonic channel add-drop multiplexer

The vertical grating resonance coupler described in Section 2 already can be utilized as a channel add/drop multiplexer between the MIM waveguide and the free space. The signal channel at the operation wavelength can be filtered out of the MIM waveguide into the free space port or can be added into the reflection port of the MIM waveguide with the injection from the free space port. To perform channel add/drop multiplexing between two separated MIM waveguides, one can place two identical vertical plasmonic resonance couplers adjacent to each other to form a novel plasmonic add-drop device as depicted in Fig. 3. The footprint of the novel add-drop device is only 13.062 μm by 1.2 μm. The input light is injected at the Port 1 of the multiplexer. It can be coupled vertically to free space by the vertical resonance coupler if the wavelength is at the operation wavelength. Through the symmetric design of the device configuration, the light will enter the upper MIM waveguide portion and eventually output at Port 3. The simulated reflection spectrum at Port 1, transmission spectrum at Port 2 and Port 4, as well as the output spectrum at Port 3 are shown in Fig. 4 for the lossless case. In the figure the specific channel wavelengths of Coarse Wavelength Division Multiplexer (CWDM) (1470, 1490, 1510, 1530, 1550, 1570, 1590, 1610 nm) are also indicated by the yellow lines. One can see that the net transmission can be as high as 75% for the ideal lossless case with a 3dB bandwidth of 6.5 nm. When the metal loss is included, the net transmission is around 0.23 with a 3dB bandwidth of 12 nm.

It is interesting to find that the free space coupling length ($L_{coupling}$) shown in Fig. 3 can affect the performance of the device. The simulated influence of $L_{coupling}$ on the coupling efficiency and the center wavelength of the device are shown in Fig. 5. We have found that when $L_{coupling}$ is shorter than two wavelengths, a large center wavelength shift or significant transmission peak splitting may occur. The optimal transmission profile demonstrated in Fig. 4 is simulated with $L_{coupling}$ = 2.54 um. The variation of center wavelength and coupling efficiency should be caused by the extra resonance occurred between the two free space ports. In principle, there are at least three resonators (2 resonance couplers + 1 extra resonance between free space ports) coupled together, which thus leads to the complicated oscillating behavior in Fig. 5 as well as the mentioned transmission peak splitting behavior exhibited in

#223864 - $15.00 USD Received 26 Sep 2014; revised 15 Dec 2014; accepted 17 Dec 2014; published 7 Jan 2015

the calculated spectra. However, one can still observe that the oscillation is more pronounced when the coupling distance is small and becomes somewhat damped when the coupling distance is increased, in particular for the center wavelength. This may be due to the diffraction effect of free space propagation, which weakens the extra resonance occurred between the two free space ports through the occurrence of a larger optical mode-mismatch loss.

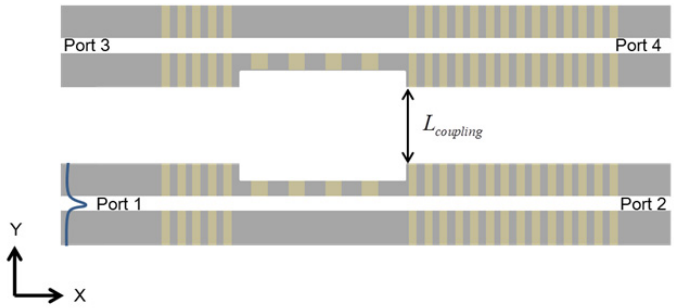

Fig. 3. Configuration of the plasmonic add-drop device, which is composed of two vertical plasmonic resonance couplers. The top coupler is the x-axis mirror image of the bottom coupler. The grating parameters are the same with those in Fig. 1.

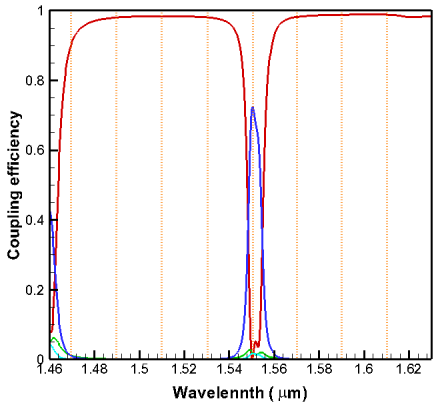

Fig. 4. Coupling efficiency for port 2(Green), port 3(Blue) and port 4(Cyan) respectively, and the reflection spectrum for port 1(Red), assuming the materials are lossless. The locations indicated by yellow lines are the CWDM channel wavelengths (1470, 1490, 1510, 1530, 1550, 1570, 1590, 1610 nm). When the metal loss is included, the transmission peak is down to 0.23 with a 3dB bandwidth of 12 nm.

#223864 - $15.00 USD Received 26 Sep 2014; revised 15 Dec 2014; accepted 17 Dec 2014; published 7 Jan 2015

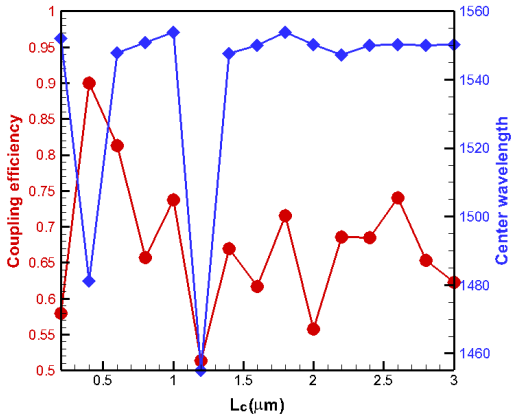

Fig. 5. Coupling efficiency at port 3 in the wavelength of 1550 nm under different lengths of $L_{coupling}$ for the lossless case

5. Conclusion

Coupling of lights from free space into the MIM plasmonic mode and vice versa is still a challenging issue because of the small overlap between the coupling modes. The studied plasmonic resonance coupler is free from this drawback with simple GC and DBR design. In this way we have demonstrated a novel wavelength selective vertical coupler capable of launching lights into plasmonic waveguides or converting lights in the plasmonic waveguide mode into free space. Under proper design, 94% of the lights in the MIM mode can be vertically coupled to free space when the metal loss is ignored. At the telecom wavelength of 1550 nm, the efficiency of the device can be around 50% when the metal loss is included in the numerical simulation. This study confirms the physical operation methodology of the device. The device can be designed to match the desired operation wavelength by optimizing different parameters including the material permittivity, sub-component lengths, and so on. A novel structure for plasmonic channel add-drop functionality has also been proposed. Two of the same vertical grating resonance couplers can be combined to form a CWDM add-drop filter with a 75% transmission peak at the operating wavelength for the ideal lossless case and close to −6dB when the metal loss is included. This approach may provide a new coupling method for plasmonic MIM waveguides under sub-wavelength confinement and find useful applications in many plasmonic researches.

Acknowledgment

The authors want to thank Prof. Din Ping Tsai and Dr. Bo Han Cheng in Research Center for Applied Sciences, Academia Sinica, Taiwan, for their help and support. And the National Center for High-Performance Computing in Taiwan is acknowledged for supporting the computation tools and facilities. This work was supported by the Ministry of Science and Technology in Taiwan under grant numbers MOST 102-2745-M-002-005-ASP and MOST 102-2221-E-009 −152 -MY3.

#223864 - $15.00 USD Received 26 Sep 2014; revised 15 Dec 2014; accepted 17 Dec 2014; published 7 Jan 2015